Separation Science and Technology

Publication details, including instructions for authors and subscription information:
http://www.informaworld.com/smpp/title~content=t713708471

Shale Oil Denitrogenation with Ion Exchange

M. E. Prudich[ab]; D. C. Cronauer[ac]; G. Marcelin[ad]
[a] Gulf Research & Development Company, Pittsburgh, Pennsylvania [b] Ohio University, Athens, OH [c] Amoco Oil Co., Naperville, IL [d] U. of Pittsburgh, Pittsburgh, PA

To cite this Article Prudich, M. E. , Cronauer, D. C. and Marcelin, G.(1987) 'Shale Oil Denitrogenation with Ion Exchange', Separation Science and Technology, 22: 2, 889 — 910
To link to this Article: DOI: 10.1080/01496398708068988
URL: http://dx.doi.org/10.1080/01496398708068988

SEPARATION SCIENCE AND TECHNOLOGY, 22(2&3), 889-910, 1987

Shale Oil Denitrogenation with Ion Exchange

M. E. PRUDICH[a], D. C. CRONAUER[b], and G. MARCELIN[c]

GULF RESEARCH & DEVELOPMENT COMPANY
P. O. BOX DRAWER 2038
PITTSBURGH, PENNSYLVANIA 15230

ABSTRACT

The nitrogen-containing aromatics normally found in crude retorted shale oils have been shown to be involved in reactions leading to the deposition of insoluble gums and sediments. These nitrogen-containing compounds must be removed in order to permit the effective utilization of the shale oil product.

A process is proposed in which the nitrogen-containing compounds found in raw shale oil are removed by mild hydrodenitrogenation followed by resin ion exchange. Ion exchange data from experimentation involving six jet fuel (154-271°C) and diesel fuel (271-343°C) boiling point cuts are presented. Amberlyst A-15, a macroreticular, strongly acidic, cation exchange resin is used in this study. Three types of experiments were performed: batch sorption equilibrium experiments, batch sorption kinetics experiments, and dynamic ion-exchange column performance tests. The Langmuir isotherm was found to describe the equilibrium sorption behavior of the shale oil/ion-exchange resin system fairly well. The sorption kinetics are described using a quadratic-driving force model.

[a] Present address: Ohio University, Athens, OH 45701
[b] Present address: Amoco Oil Co., Naperville, IL 60566
[c] Present address: U. of Pittsburgh, Pittsburgh, PA 15261

Dynamic modeling, assuming intraparticle (solid) diffusion control and including the results of the batch equilibrium and batch kinetics experiments, provides reasonable prediction of the results of dynamic ion-exchange column performance tests.

Two additional resins (Amberlyst XE-397 and Amberlyst XN-1010) of similar chemical composition to Amberlyst A-15, but with 1/3 and 3 times the degree of crosslinking, respectively, were tested. Pore size distributions were determined for each of the three resins. The resin with the largest average pore size was shown to have an effective capacity for nitrogen-containing compounds of about 2.5 times the next most effective resin.

INTRODUCTION

The nitrogen-containing aromatics normally found in crude retorted shale oils have been shown to be involved in reactions leading to the deposition of insoluble sediments and gums[1]. These nitrogen-containing compounds must be removed in order to permit the effective utilization of the shale oil product. Severe hydrodenitrogenation is the means most commonly used to reduce the concentration of these nitrogen-containing compounds from their initial levels (1.3 to 2.2 wt% N) to reasonable levels (<50 ppm). As such, hydrodenitrogenation has been the subject of considerable research[2,3].

Substantial effort has been devoted to elucidating the mechanism of the hydrodenitrogenation reaction, principally because copious amounts of expensive hydrogen are typically consumed during this heteroatom removal process. Early work by Koros et al.[4] revealed that saturation preceded ring cleavage and eventual nitrogen removal as ammonia. Effects of method of shale oil extraction from the rock on processing results[5], variations in the processing methods themselves[6], and properties of catalysts used for the hydrotreating[7] have drawn the attention of researchers in the attempt to reduce this technical possibility to commercial reality.

A second, and nearly separate, body of literature has been developed around the removal of nitrogen-containing compounds in non-aqueous media by methods such as ion exchange and solvent extraction. Much of this work has centered around the development of analytical methods. Comparisons of various methods of separation[8,9], comparison of ion exchangers[10,11,12], and a review of a variety of analytical approaches[13] will acquaint the reader with this field. Work with model compounds has helped to elucidate how an ion-exchange approach may be applied to fuels[14,15], while work with actual feedstocks such as bitumen and heavy oil has helped to identify what difficulties may be encountered during actual operations[16,17].

A linkage between the two approaches described above is supplied by researchers who are aware of the significant cost of hydrogen for refining operations and who wish to take advantage of the generation of basic molecules during the partial hydrotreating of shale oil. Work by Parkinson[18] has described the approach of hydrotreating followed by acid extraction. Cronauer et al.[19] have demonstrated the utility of combining the hydrotreating step with resin ion exchange. This two step processing of shale oil for nitrogen removal appears to be particularly attractive because while the unit cost of removing each incremental amount of nitrogen-containing compound by hydrodenitrogenation increases as the concentration of the nitrogen-containing compounds in the shale oil becomes small, the ion exchange process becomes increasingly effective (both technically and economically) in this same concentration region.

The present investigation has been designed to provide a preliminary evaluation of the effectiveness of resin ion exchange as a technique for the removal of nitrogen-containing compounds from mildly hydrodenitrogenated shale-derived liquids. The first part of this study deals with the performance of a single ion-exchange resin, Amberlyst A-15. The goal of this part of the work is the identification of a simple, asymptotic model which can be used to describe the ion-exchange behavior of this system. The formulation of such a model should provide a preliminary screening tool for data analysis as well as point the way towards process and/or chemical improvements. The experimental data currently available do not justify the formulation of more detailed mechanistic models for the removal of nitrogen-containing molecules from shale oil by resin ion exchange.

The second part of this paper deals with a comparison of the performance of the Amberlyst A-15 ion-exchange resin with two other resins (Amberlyst XN-1010 and Amberlyst XE-397). The two resins, XN-1010 and XE-397, have essentially the same chemical functionality as the A-15 resin, but with 3 times and 1/3 times the degree of crosslinking, respectively. The degree of crosslinking is shown to effect the internal structure of the ion-exchange resins. In ion-exchange processes, the physical as well as the chemical aspects of the sorption process must be understood in order to maximize the utility of the system. When large molecules are involved in ion exchange, the physical constraints imposed by their diffusion may control the process. Thus, knowledge of the transport properties of the molecule/resin systems involved is necessary to the understanding of the ion-exchange process and interpretation of the observed phenomena.

The diffusion of molecules into liquid-filled pores is the relevant problem in the case of nitrogen-compound removal from shale oil by resin ion exchange. A thorough understanding of the transport of liquids in porous media is important in predicting exchange rates and in choosing solid adsorbents. Prasher and Ma[20] reported the diffusivity of molecules into liquid-filled substrates and developed some correlations between diffusivities, molecular radius, and pore

radius. A few experimental or theoretical studies have reported diffusion limitations of large molecules into porous media. Shirura et al.[21] studied the diffusion behavior of large molecules into catalyst pores and correlated transport properties with hydrotreating activity for different pore structures. Baltus and Anderson[22] studied the diffusion of asphaltene fractions through microporous membranes of carefully controlled pore size and found a discrepancy with theory which they attributed to molecular shape. Other investigators have shown that it does not suffice to calculate effectiveness factors from existing theories, since parameters such as pore shape, molecular shape, and pore network structure cannot be satisfactorily taken into account[23]. Furthermore, other phenomena such as "skin effects", small surface openings covering large internal pores, cannot be predicted à priori.

A number of techniques exist for measuring or estimating the physical constraints of diffusion into pores. The easiest, and unfortunately one of the least meaningful methods, consists of measuring pore size distributions by either nitrogen sorption or mercury porosimetry. Average pore size and pore size distributions determined by these techniques often rely on the assumption that the solid particle contains cylindrical pores which can be completely filled. As such, these techniques completely neglect the effects that pore shape can have on the effective intraparticle diffusivity.

EXPERIMENTAL

Shale Oil Feed

The shale oil distillate used in this study was prepared by mildly hydrotreating and subsequently distilling a raw shale oil. The raw shale oil was an available sample of Occidental Oil from Burn Number 6. The raw shale oil (1.37 wt% N) was hydrodenitrogenated at three levels of severity over a commercial catalyst (NM-504, Katalco Corporation). The three product oils were designated P67-152 (0.51 wt% N), P67-153 (0.30 wt% N), and P67-154 (0.15 wt% N), respectively. The raw oil and the product oils were then fractionated by distillation into the following cuts:

Naphtha	OP - 154°C
Jet Fuel	154 - 271°C
Diesel Fuel	271 - 343°C
Gas Oil	343 - 516°C
Residue	516°C+

The product inspections for the raw shale oil and the hydrotreated products are given in Table 1. Only the jet fuel and the diesel fuel cuts are discussed in this paper. A more detailed description of the sample preparation and analyses of the feedstocks can be found in a report by Cronauer(24). Total nitrogen in the shale oil fractions was

analyzed by oxidative combustion followed by chemiluminescence detection. A D-10 Total Nitrogen Analyzer System (Dohrman Division, Environtech Corporation, Santa Clara) was used for this analysis. All nitrogen contents are reported on a weight/weight basis (example - grams nitrogen per gram resin; grams nitrogen per gram oil). All values concerning the ion-exchange resin are given on a dry basis.

Adsorbent(Ion-Exchange Resin)

Amberlyst A-15 (Rohm & Haas, Philadelphia) was used exclusively throughout the first set of experiments. A-15 is a macroreticular, strongly acidic, cation exchange resin. Chemically, it is a sulfonated, crosslinked styrene/divinylbenzene polymer. Amberlyst A-15 is described as having an exchange capacity of 4.4 meq/g, an internal surface area of 100 m2/g, and an average pore diameter of 160 Å. The exchange capacity of 4.4 meq/g should give Amberlyst A-15

TABLE 1

Properties of Shale Oil Samples

Elemental Analysis, Wt%	Raw Raw Shale Oil	P67-152	P67-153	P67-154
Carbon	84.64	85.91	86.55	86.07
Hydrogen	11.82	12.92	13.16	13.19
Nitrogen	1.37	0.51	0.30	0.15
Sulfur	0.71	0.04	0.04	0.02
Distillation Yields, Wt%				
OP - 154°C	0.0	1.3	1.4	1.5
154 - 271°C	16.9	22.3	24.2	25.5
271 - 343°C	22.7	26.9	27.1	27.6
343 - 516°C	46.6	43.0	42.5	41.9
516°C+	13.8	6.2	4.4	2.6
Losses	----	0.3	0.4	0.9
Distillate Nitrogen, Wt%				
OP - 154°C	----	----	----	----
154 - 271°C	----	0.27	0.17	0.09
271 - 343°C	----	0.46	0.28	0.14
343 - 516°C	----	0.58	0.35	0.18
516°C+	----	----	----	----

Table 2

Ion-Exchange Resin Properties

Resin	Exchange Capacity, meq/g*	Cap. Util., %	Surface Area, m^2/g	Ave. Pore Radius, Å	Pore Vol., mL/g	Cross-linking, ----*	D_{eff}, cm^2/s
XN-1010	3.6	53	200	60	0.46	3	0.30×10^{-8}
A-15	4.4	53	100	160	0.48	1	1.55×10^{-8}
XE-397	4.9	104	66	300	0.50	0.33	1.86×10^{-8}

* Values supplied by Rohm & Haas; crosslinking values are relative only; Cap. Util. = theoretical exchange capacity utilized at the ratio of one nitrogen atom per exchange site.

the ability to adsorb 0.062 grams of nitrogen per gram of dry resin if all of the sites are utilized at the ratio of one nitrogen per site. The ion-exchange resins, Amberlyst XE-397 and Amberlyst XN-1010, used in the second part of the study are chemically similar to Amberlyst A-15 but have 1/3 and 3 times the degree of cross-linking, respectively. Pertinent ion-exchange resin properties for these two resins can be found in Table 2. The nitrogen-removal effectiveness of 19 additional adsorbents can be found elsewhere(24).

Sorption Equilibrium Experiments

Equilibrium resin loading data were generated for the six jet fuel and diesel fuel fractions. In order to obtain these data, 15 gram samples of the shale oil fraction to be studied were weighed into each of several small Erlenmeyer flasks. Various amounts (0.25, 0.5, 1.0, 2.0, 3.0, 4.0 grams) of resin had previously been added to the flasks. The oil and resin were maintained at 27°C for about 72 hours during which time the flasks were continuously swirled. (Longer treatment times confirmed that no additional sorption occurred after 72 hours). At the end of the 72 hour period, the oils were filtered to remove the ion-exchange resin and the filtrate (shale oil) was analyzed for nitrogen content. The amount of nitrogen adsorbed by the ion-exchange resin was calculated by difference. Resin nitrogen levels were not measured directly. Desorption/regeneration data were also generated. These desorption data can be found in reference 24.

Sorption Kinetics Experiments

Intraparticle diffusion dynamics were studied by observing the rate at which the nitrogen-containing compounds were taken up by the resin in a well-mixed tank. Care was taken to insure that sufficient mixing energy was used so that only diffusion within the resin

particle would control the sorption rate process. In a typical experiment, 10 grams of ion-exchange resin were weighed into a baffled, glass mixing vessel along with 200 ml of the shale oil fraction to be studied. The shale/oil resin mixture was then mixed at stirrer speeds of 320-340 rpm for 24 hours. Small samples of shale oil liquid were taken periodically throughout the run and analyzed for nitrogen content. The sample sizes were kept small so as not to cause a significant decrease in the volume of liquid being agitated.

Dynamic Column Performance

A set of dynamic ion-exchange runs was made using the Amberlyst A-15 resin. In these runs, about 30 grams of fresh(dry) resin were charged to a 9.5 mm-i.d. by 1000 mm-length tube. The shale oil fractions were then pumped through the resin bed at a fixed flow rate. Samples of the effluent shale oil product were taken and analyzed for nitrogen content.

Mercury Porosimetry

The pore size distributions of the ion-exchange resins were determined using a Micromeritics Scanning Mercury Porosimeter capable of operating to 60,000 psig, thereby measuring pores in the range of 20 to 5000 Å in radius.

RESULTS AND DISCUSSION

Several simplifying assumptions are inherent in the analysis and discussion of the data presented below. These assumptions are:

- The dynamic ion-exchange process for nitrogen-compound removal from shale oil is intraparticle (solid) diffusion controlled.
- All nitrogen-containing species within a given fraction (boiling range cut and/or degree of hydrodenitrogenation) can be accurately described by a single, average effective diffusivity and a single, average set of equilibrium parameters.
- The ion-exchange resin beads (for each resin type) can be accurately described by a single, average particle radius.
- The sorption of nitrogen-containing compounds is a reversible process.

These assumptions have been made in order to simplify the mathematical treatment of the data. The batch sorption kinetics experiments have been controlled in such a way so as to insure particle side resistance control. The decision to include only intraparticle (solid) diffusion in this analysis of the ion-exchange

data is based on observation of the shapes of the dynamic ion-exchange column breakthrough data. These data show that the breakthrough curves are markedly asymmetric with distinct tailing. These shape attributes tend to be characteristic of ion-exchange systems where intraparticle (solid) diffusion is the rate controlling step. It can be argued that pore diffusion should be a significant contributor to the particle-side resistance for the case of a macroreticular resin. Our data will later show that this is almost certainly true in the case of nitrogen-compound removal from shale-derived liquids.

The equilibrium sorption data generated for all six shale oil fractions were analyzed assuming that they could be represented by simple, monovariant isotherms having constant separation factors. Using an approach described by Vermeulen et al.(25), a fit was made of each individual set of data to the equation,

$$y^* = \frac{x}{r + x - rx} \qquad (1)$$

where y^* and x are dimensionless solid and liquid phase solute concentrations, and r is the separation factor. When $r<1$, the equilibrium isotherm is favorable to the uptake of the solute and the isotherm is a Langmuir isotherm. When $r=1$, the isotherm is linear (Raoult's law), while the condition $r>1$ describes the Freundlich isotherm (unfavorable to the uptake of solute). Values for r as determined for the six shale oil fractions can be found in Table 3. Since $r<1$ for all of the shale oil fractions tested, the Langmuir isotherm was used. The Langmuir isotherm can be described as,

$$q^* = \frac{QK_Lc}{(1 + K_Lc)} \qquad (2)$$

where Q is the maximum asymptotic solid-phase solute concentration, K_L is the equilibrium constant, and q^* and c are the solid and liquid phase solute concentrations, respectively. Estimates for the terms Q and K_L are also given in Table 3. Figures 1 and 2 show the experimental data plotted about Langmuir isotherms generated for the jet fuels and diesel fuels, respectively.

A perusal of Table 3 shows that the percent of the potential resin capacity of 0.062 g N/g resin which is utilized at saturation ranges from a high of 92 percent (0.057 g N/g resin) for P67-154 jet fuel (0.09 wt% N) to a low of 26 percent (0.016 g N/g resin) for P67-152 diesel fuel (0.46 wt% N). Simply put, the utilization of sorption capacity of Amberlyst A-15 for nitrogen-containing species decreases with increasing boiling range of the shale oil fraction (jet fuel > diesel fuel) and increases with decreasing nitrogen content (increasing severity of hydrodenitrogenation) within a given boiling range fraction (P67-152 < P67-153 < P67-154). These

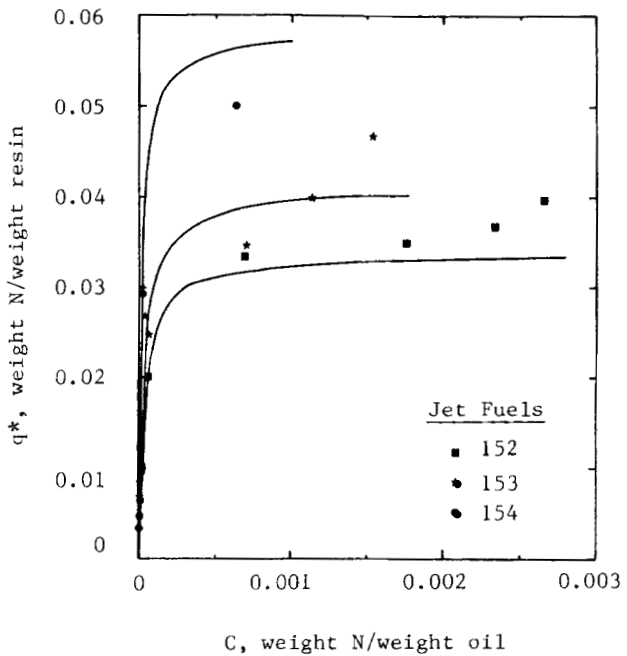

FIGURE 1. Jet fuel equilibrium sorption curves.

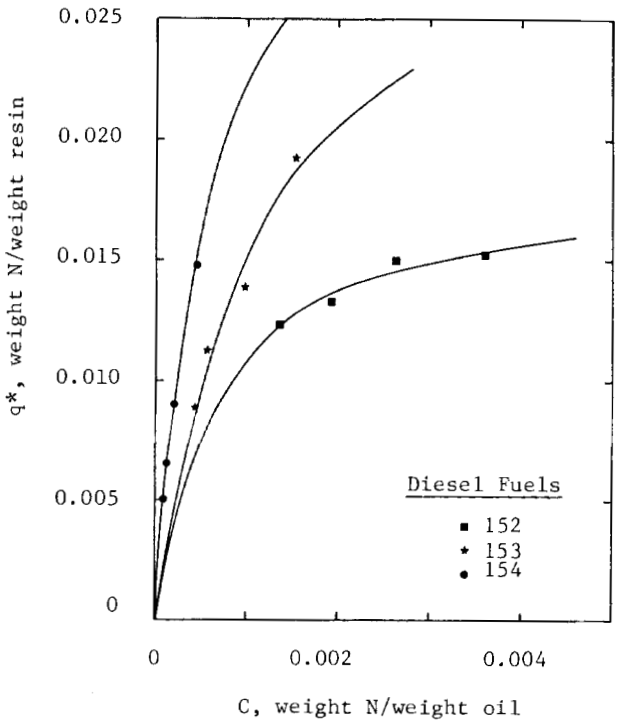

FIGURE 2. Diesel fuel equilibrium sorption curves.

(Solid lines are least square fits to the linearized Langmuir isotherm; c is the liquid-phase solute concentration; q^* is the solid-phase solute concentration in equilibrium with c.)

Table 3

Sorption Parameters for Amberlyst A-15

Fuel	r, ---	q_{ref}, g N/ g resin	c_{ref}, g N/ g oil	Q, g N/ g resin	K_L, ---	Cap. Util., %	D_{eff}, cm^2/s
Jet Fuels							
P67-152	0.011	0.033	0.00280	0.0332	31900	53	1.59×10^{-8}
P67-153	0.018	0.040	0.00178	0.0409	30100	64	0.78×10^{-8}
P67-154	0.022	0.057	0.00090	0.0566	51000	92	---
Diesel Fuels							
P67-152	0.131	0.016	0.00460	0.0183	1450	26	---
P67-153	0.295	0.023	0.00280	0.0329	840	37	---
P67-154	0.293	0.025	0.00140	0.0353	1730	40	---

Cap. Util. = percent of theoretical exchange capacity utilized at the ratio of one nitrogen atom per exchange site.

observations indicate that it is not possible for Amberlyst A-15 to sorb one N for each ion-exchange site for all of the shale oil fractions studied. Apparently, all of the sorptive sites are not available for ion exchange with all of the nitrogen-containing compounds. This lack of efficiency could be caused by the steric blocking of adjacent sites by large, sorbed molecules; the exclusion of some of the larger nitrogen-containing molecules from the smaller pores; the fouling and plugging of the resin by some unidentified fraction in the shale oil; or some other change to the resin caused by exposure to the oils.

Ion-exchange sorption kinetics were determined for only two of the six shale oil fractions, P67-152 jet fuel and P67-153 jet fuel. The experimental data obtained for the other jet and diesel fuel fractions were not suitable for evaluation by the mathematical methods employed because the ion-exchange column was too short to permit a "constant pattern" sorption front to develop for these fractions. The raw data for these runs can be found elsewhere(24). The quadratic-driving-force relation(26) was used to describe the kinetics of ion exchange in the analysis of the batch rate data. Hall et al.(27) have shown that the quadratic-driving-force relationship adequately approximates the rigorous numerical solution for

solid-diffusion kinetics under constant pattern conditions. The quadratic-driving-force expression can be represented as,

$$\frac{d\bar{q}}{dt} = \frac{D_{eff}\pi^2}{r_o}\left(\frac{\bar{q}^{*2} - \bar{q}^2}{2\,\bar{q}}\right) \qquad (3)$$

where t is the time, D_{eff} is the effective intraparticle diffusivity, and r_o is the ion-exchange resin bead radius. The $\bar{q}$ values represent the solid-phase solute concentration averaged over the volume of the ion-exchange resin bead.

In order to determine the effective diffusivities, experimental data were least square fit to the quadratic-driving-force equation keeping mass balance considerations in mind. An iterative, finite difference technique was used to perform the least squares fitting. An average value of 0.0447 cm was assigned to r_o in order to arrive at numerical values for D_{eff}. The experimental values plotted against the least square curves are shown in Figure 3. The curve for the P67-153 jet fuel illustrates the excellent experimental reproducibilty obtained for these data. This curve includes data from three different batch rate experiments.

The effective diffusivity for the nitrogen-containing compounds in Amberlyst A-15 was found to decrease from 1.59 x 10^{-8} cm^2/s for P67-152 jet fuel to 0.78 x 10^{-8} cm^2/s for P67-153 jet fuel. When these two numerical values are considered in light of the qualitative observations made for the other four shale oil fractions, a distinct pattern emerges. The effective diffusivity within the ion-exchange resin decreases with increasing boiling range of the shale oil fraction (jet fuel > diesel fuel). This observation can be explained in terms of the larger molecular size of the nitrogen-containing compounds found in the diesel fuel fraction(24). However, within the same boiling range fraction, the effective diffusivity into the resin bead is seen to decrease with decreasing nitrogen-compound content. This observation of decreasing effective diffusivity with decreasing liquid-phase solute concentration is consistent with theoretical analyses of diffusion in porous solids made by other investigators(28,29). When dealing with porous solids, the effective intraparticle diffusivity can be thought of as being comprised of the sum of two terms. One term, which includes the solid-diffusivity (diffusivity of the solute through the solid surface) can usually be considered to be constant. The other term, which includes the pore-diffusivity (diffusivity of the solute within the liquid-filled pores of the particle) can be shown to decrease with decreasing bulk liquid-phase solute concentration. The net action of these two terms results in an effective intraparticle diffusivity that decreases with decreasing liquid-phase solute concentration.

The mathematical treatment of the continuous-flow ion-exchange column (breakthrough curve) data is handled differently from that for the equilibrium and rate data. The analysis of the batch equilibrium

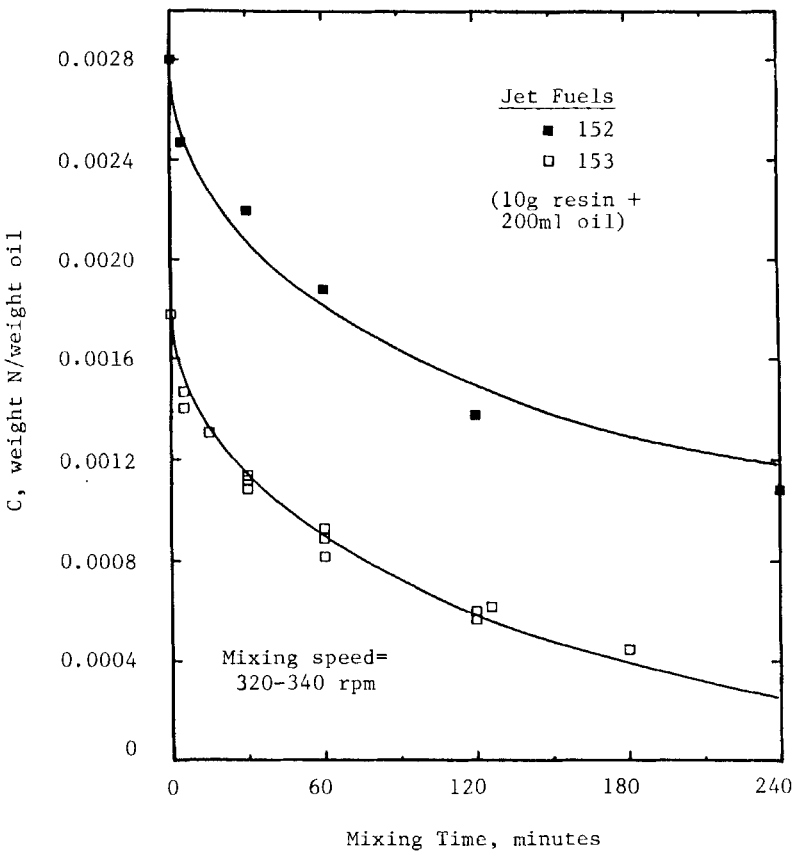

FIGURE 3. Jet fuel sorption rate experiments in a mixed tank. (Solid lines are least square fits to the quadratic-driving-force rate relationship; C is the liquid-phase solute concentration.)

and rate data was made by statistically curve fitting the data to assumed mathematical forms. The continuous column behavior is analyzed by utilizing the results of the equilibrium and rate data analyses to generate breakthrough curves that are therefore derived independently of the continuous flow data. The predicted breakthrough curves were generated by solving an equation based on applying the quadratic-driving-force rate expression to fixed bed ion-exchange systems with favorable ion-exchange equilibria(27). The modeling equation is given as,

$$\frac{1}{(1-r)}\left[\ln\frac{(1+r)-2rx_1-(1-r)x_1}{(1+r)-2rx_2-(1-r)x_2}+r\ln\left\{\frac{1-x_1}{1-x_2}\cdot\frac{x_2+\left(\frac{1+r}{1-r}\right)}{x_1+\left(\frac{1+r}{1-r}\right)}\right\}+2r\ln\left(\frac{x_2}{x_1}\right)\right]$$

$$=\Psi_q N_{PF}\,(T_2-T_1) \qquad (4)$$

where $\Psi_q N_{PF}$ is the corrected number of transfer units(27) and T is the ratio of the actual volume of column effluent to the stoichiometric amount of effluent that would be required to bring the resin bed into equilibrium with the feed stream if all of the nitrogen-containing compounds were adsorbed. The subscripts 1 and 2 indicate two different treatment volumes. The solutions of Equation 4 for the P67-152 and P67-153 jet fuels along with experimentally determined breakthrough curve data are shown in Figures 4 and 5, respectively.

The fit of the experimental data to the model curves is reasonably good for the middle portions and the tails of the breakthrough curves for both P67-152 and P67-153 jet fuels. However, both oils show premature breakthrough at the leading edge of the breakthrough curve. This premature breakthrough could be due to any one, or combination of, the following reasons: undeveloped concentration front, concentration dependent diffusivity, partial channeling, and/or chromatographic separation of the nitrogen-containing species in the shale oil. The concentration dependent intraparticle diffusivity, due to the contribution of pore diffusion to the overall effective rate, is most likely one contributing cause of this deviation from the simple model.

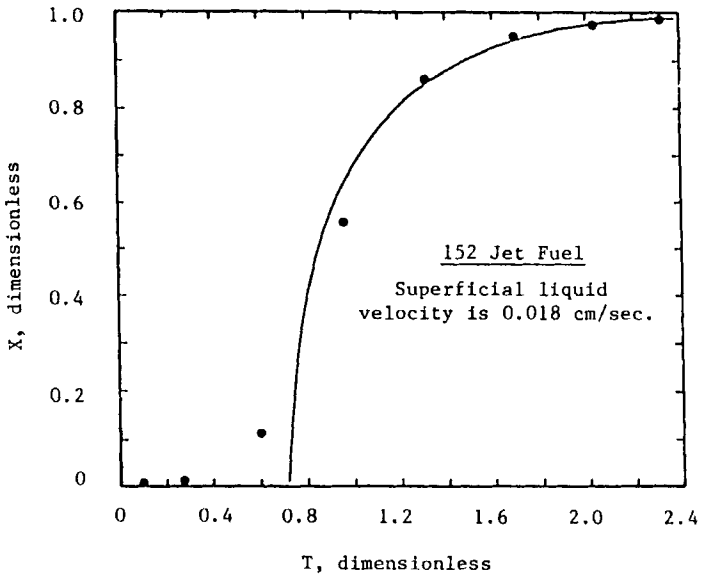

FIGURE 4. Dimensionless ion-exchange breakthrough curve for 152JET. (The solid line is the predicted breakthrough curve assuming intraparticle, solid-phase diffusion control.)

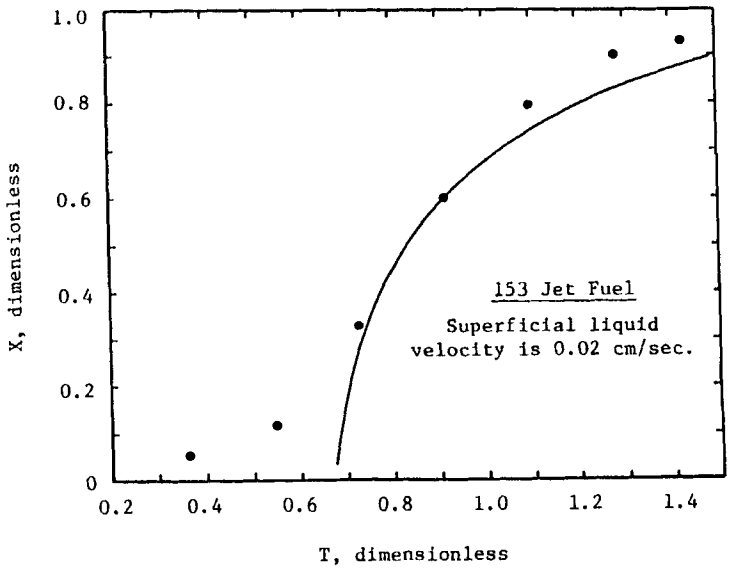

FIGURE 5. Dimensionless ion-exchange breakthrough curve for 153JET. (The solid line is the predicted breakthrough curve assuming intraparticle, solid-phase diffusion control.)

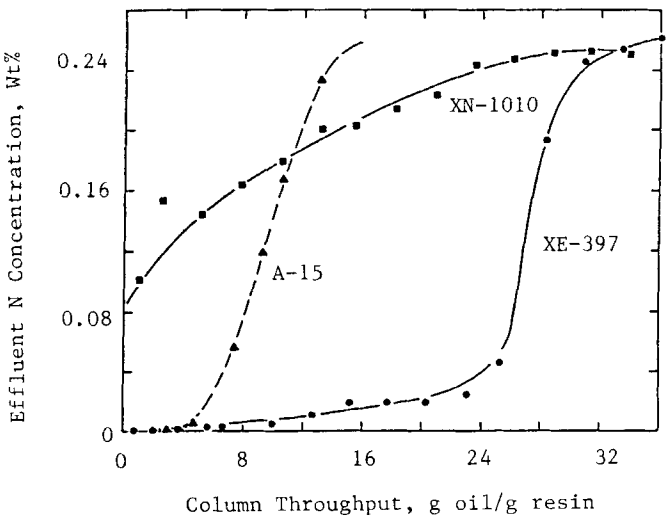

FIGURE 6. Comparison of breakthrough curves for XN-1010, A-15, and XE-397 resins using 152JET containing 0.27% N.

Armed with the testing methodology developed for Amberlyst A-15, it was decided to investigate the effects of varying the resin pore structure on the nitrogen-containing compound ion-exchange sorption performance. Resin pore morphology was a logical variable to pursue as the nitrogen-removal ion-exchange process appeared to be controlled by diffusion within the resin bead. Amberlyst XN-1010 and Amberlyst XE-397 were selected for this study since they were known to vary from Amberlyst A-15 primarily in degree of crosslinking (3 times and 1/3 times, respectively). Because of a short supply of P67-153 and P67-154 jet fuels, it was necessary to test the samples of Amberlyst XE-397 and Amberlyst XN-1010 using only P67-152 jet fuel. As shown in Figure 6, the XE-397 is far superior to A-15 and XN-1010 in removing nitrogen-containing compounds from the P67-152 jet fuel. In terms of integrated nitrogen sorption capacity in column operation, the Amberlyst XE-397 resin was about 2.5 times better than the Amberlyst A-15 resin.

That this improved performance was due to an increase in ion-exchange capacity was confirmed by a more detailed analysis of the ion-exchange equilibria. The results of these studies are shown in Figure 7. Assuming Langmuir-type sorption isotherms, Amberlysts XE-397, A-15, and XN-1010 show capacities of 0.072, 0.033, and 0.027 grams N/gram resin, respectively. When considering their theoretical exchange capacities (4.9, 4.4, and 3.6 meq/gram), this corresponds to

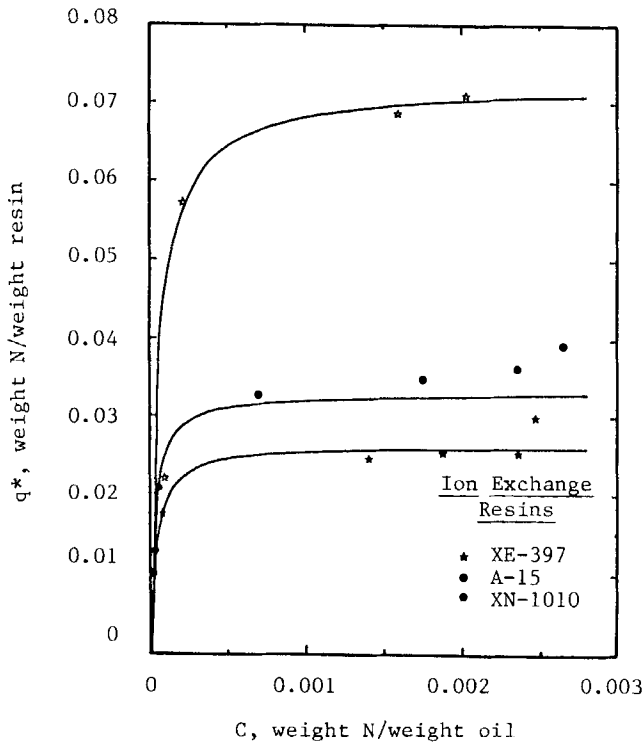

FIGURE 7. P67-152 jet fuel equilibrium sorption curves. (Solid lines are fits to the linearized Langmuir isotherm; c is the liquid-phase solute concentration; q^* is the solid-phase solute concentration in equilibrium with c.)

a capacity utilization of 104% for XE-397 and only 53% for both A-15 and XN-1010. Therefore, it is likely that a mechanism such as pore-mouth plugging is making some of the reaction sites unavailable for ion exchange with the nitrogen-containing compounds.

Experiments were also run to determine the rate of nitrogen removal in a batch tank. The results of these tests are presented in Figure 8. Assuming that intraparticle diffusion is controlling and that the rate of ion exchange can be described by a quadratic-driving-force expression, effective diffusivities for the nitrogen-compound removal ion-exchange process can be calculated. The effective diffusivities determined in this manner for XE-397, A-15, and XN-1010 are 1.86×10^{-8}, 1.55×10^{-8}, and 0.30×10^{-8} cm^2/s, respectively. Even though XE-397 and A-15 have similar effective diffusivities, XE-397 adsorbs nitrogen-containing compounds much faster than A-15 because of its superior sorption capacity.

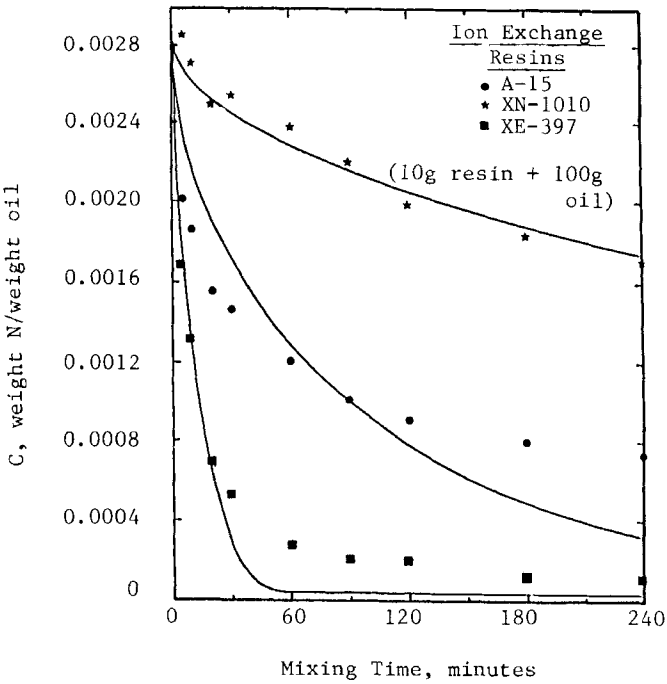

FIGURE 8. Ion-exchange sorption kinetics results for XN-1010, A-15, and XE-397 resins with 152JET containing 0.27%N. (Solid lines are least square fits to the quadratic-driving-force rate relationship; c is the liquid-phase solute concentration.)

Pore size distributions for XN-1010, A-15, and XE-397, as determined by scanning mercury porosimetry are shown in Figure 9. Although all three resins show approximately the same total pore volume (ca. 0.5 mL/gram), the pore size distributions are significantly different in all three cases. The XN-1010 resin shows a distribution of pores over most of the micro-pore range, 20 to 400 Å, with little porosity in the macro-pore region. The A-15 resin is intermediate-pored, with most of the pore volume present in 40 to 1000 Å radii pores. Almost no pores smaller than 40 A are present in this resin. The pore size distribution of XE-397 shows this resin to consist of the largest pores, mostly greater than 100 Å and a significant portion above 500 Å.

A prominent feature of the porosimetry results is the hysteresis that is observed for all of the intrusion-extrusion curves. Although

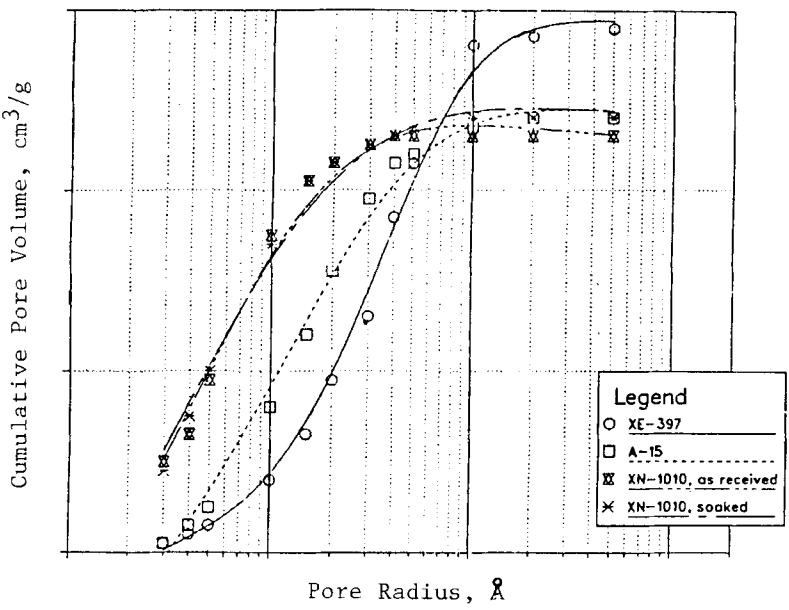

FIGURE 9. Cumulative pore volume versus log of pore radius for the XN-1010, A-15, and XE-397 resins.

this hysteresis is noticeable for both the XN-1010 and A-15 resins, it is much more pronounced for the XE-397 resin. This large hysteresis for the Amberlyst resins might imply that they possess an unusual pore structure not consisting of simple, cylindrical,and interconnecting pores. Rather, it could indicate the presence of either "ink-well" pores or a complicated network of throats and cavities which result in an easy-to-fill but difficult to empty material. The large intrusion-extrusion hysteresis could also be indicative of structural changes of the resin particles by the large mercury pressure. To investigate this possibility, three consecutive intrusion-extrusion scans were performed on the same sample of XE-397 resin. Within experimental error, the curves were identical (pore volume to ± 0.05 mL) and in all cases the hysteresis was evident. Since the resin was not damaged irreversibly, the hysteresis was most likely due to pore morphology and not to resin destruction. "Ink-well" pores would be expected to contribute a diffusional limitation in excess of that due to pores of equal volumetric equivalent diameter because of the presence of narrow pore restrictions between the larger internal cavities. This added diffusional resistance in the large pored XE-397 resin would help to

explain why the XE-397 resin and the A-15 resin have similar effective diffusivities but widely different sorption capacities. The surface areas of the resins (as presented in Table 2) were calculated from the mercury intrusion curves assuming cylindrical pores and complete filling and are, therefore, only approximate.

SUMMARY/CONCLUSIONS

The effectiveness of a combined process consisting of mild hydrodenitrogenation followed by a resin ion-exchange treatment of low boiling shale oil distillates has been demonstrated. A simple, asymptotic model based on the Langmuir sorption isotherm and the assumption of intraparticle solid-phase diffusion control is adequate to guide resin performance screening. The use of this simple model provides a way of numerically estimating resin sorption capacities and effective intraparticle diffusivities (and rates of ion exchange). Observations of the parametric variations of these estimated capacities and diffusivities may lead to the development of more accurate and comprehensive mechanistic models.

Work with the Amberlyst A-15 resin has suggested nitrogen-compound size and shape as important parameters in the nitrogen-compound-removal ion-exchange process. Amberlyst A-15 shows a higher equilibrium capacity utilization for nitrogen-containing compounds found in the lower boiling jet fuel fraction than it does for nitrogen-containing compounds found in the higher boiling diesel fuel fraction. The molecular weights of compounds found in the jet fuel fraction are expected to be smaller than those for compounds found in the diesel fuel fraction. Further evidence for the influence of molecular size/shape can be gained from the fact that, within a given boiling point fraction (either jet or diesel), the equilibrium sorption capacity of Amberlyst A-15 increases with increasing degree of hydrodenitrogenation. The nitrogen-containing compounds within a given boiling point grouping would be expected to decrease in effective molecular diameter (due to ring cleavage and/or loss of pendant groups) with increases in the severity of hydrodenitrogenation.

The set of experiments utilizing Amberlyst resins XN-1010, A-15, and XE-397 and P67-152 jet fuel has identified resin pore morphology as a key performance-controlling variable. Amberlysts XN-1010, A-15, and XE-397 have mean pore radii of 60 Å, 160 Å, and 300 Å, respectively. If it is assumed that one nitrogen-containing group can be adsorbed at each ion-exchange site, Amberlysts XN-1010 and A-15 show sorption of only 53% of their theoretical capacities. Amberlyst XE-397 shows sorption of 104% of its theoretical capacity. This observation would suggest that pores below a certain size range are not available to nitrogen-compound ion-exchange. The presence of these small pores result in underutilization of the exchange capacity of the resin. Pore morphology also is shown to influence the

magnitude of the effective intraparticle diffusivity. The small pored XN-1010 resin shows an effective intraparticle diffusivity of 0.30×10^{-8} cm^2/s, while the intermediate pored A-15 and large pored XE-397 resins show effective intraparticle diffusivities of 1.55×10^{-8} cm^2/s and 1.86×10^{-8} cm^2/s, respectively. The similarity in magnitude of the diffusivities in the intermediate and large pored resins may be due to the presence of "ink well" pores (large pores with constricted necks) in the large-pored Amberlyst XE-397 resin. These physical restrictions in the pore structure of XE-397 would be expected to decrease the magnitude of pore diffusivity within this resin.

The effective intraparticle diffusivity for each of the resins studied is probably a combination of solid- and pore-phase diffusivities. The inclusion of pore-diffusivity as a component of the effective diffusivity would help explain the observed concentration dependence of the effective intraparticle diffusivity (decrease in effective intraparticle diffusivity with decreasing liquid-phase solute concentration). This would resolve the variation between experimental observation and model prediction evidenced in Figures 4, 5, and 8.

ACKNOWLEDGEMENTS

The authors would like to acknowledge the financial support of both the United States Department of Energy (Contract No. DE-AC17-80BC10313) and Gulf Research and Development Company.

NOMENCLATURE

- c = concentration of solute in the liquid phase, g N/g oil
- c_{ref} = concentration of solute in the liquid-phase feed, g N/g oil
- D_{eff} = effective intraparticle diffusivity based on the quadratic-driving-force expression, cm^2/sec
- K_L = Langmuir sorption equilibrium constant, dimensionless
- q^* = concentration of solute in the solid phase in equilibrium with c, g N/g resin
- q_{ref} = concentration of solute in the solid phase in equilibrium with cref, g N/g resin
- q = volume averaged solid-phase solute concentration, g N/g resin
- Q = asymptotic solid-phase solute concentration, g N/g resin
- r = separation factor, $r = x_i y_j / x_j y_i$, dimensionless
- r_o = average resin bead radius, cm
- t = time, sec

T = $c_{ref}(V - v\epsilon)/q_{ref}\rho_b v$, throughput parameter, dimensionless
v = volume of the resin bed, cm^3
V = cumulative fluid volume fed to the column, cm^3
x = c/c_{ref}, liquid-phase solute concentration, dimensionless
y^* = q^*/q_{ref}, solid-phase solute concentration, dimensionless

ϵ = bed voidage
ρ_b = ion-exchange resin bulk density, g/cm^3
$\psi_q N_{PF}$ = corrected number of transfer units, dimensionless

REFERENCES

1. J.V. Cooney, E.J. Beal, and R.N. Hazlett, Prepr. Div. Fuel Chem., Am. Chem. Soc., 29(3), 247(1984).
2. R.E. Poulson, Prepr. Div. Fuel Chem., Am. Chem. Soc., 23(6), 825(1975).
3. A. Akgerman, and R.G. Anthony, "Hydrodenitrogenation: State of the Art and New Catalysts," 1983 AIChE Annual Meeting, #27d, Washington, D.C., 1983.
4. R.M. Koros, S. Bank, J.E. Hofmann, and M.I. Kay, Prepr. Div. Petrol. Chem., Am. Chem. Soc., 12(4), B165(1967).
5. S.A. Holmes, and L.F. Thompson, "Nitrogen-Type Distribution in Hydrotreated Shale Oils. Correlation with Upgrading Process Conditions," 14th Oil Shale Symposium Proceedings, 235, Golden, CO, 1981.
6. R.F. Sullivan, and B.E. Strangeland, Advances in Chemistry Series, No. 179, Am. Chem. Soc., 25(1979).
7. J.R. Katzer, H. Kwart, and A.B. Stiles, "Development of Superior Denitrogenation and Isomerization Catalysts for Processing Crude Oil Derived from Shale. Part II. Final Report," NTIS Report No. AD-A-111559/1, 1981.
8. P. Burchill, A.A. Herod, J.P. Mahon, and E. Pritchard, Chromatogr., 265(2), 223(1983).
9. V.L. Rapoport, and N.V. Razumov, Neftekhimiya, 23(6), 825(1983).
10. R.M. Carlyle, PT-Procestech., 38(1), 34(1983).
11. P.V. Webster, J.N. Wilson, and M.C. Franks, Anal. Chim. Acta, 38(1-2), 193(1967).
12. C.A. Audeh, Ind. Eng. Chem. Prod. Res. Dev., 22(2), 276(1983).
13. K.H. Altgelt, and T.H. Gouw, Adv. Chromatogr., 13, 171(1975).
14. M. Stejskal, G. Sebor, and O. Weisser, Ropa Uhlie, 23(11), 647(1981).
15. M. Caude, C. Bollet, R. Rosset, and P. Sassiat, Analysis, 4(9), 427(1976).

16. H. Sawatzky, S.M. Ahmed, A.E. George, and G.T. Smiley, CANMET Rep., 77-10, 1977.
17. V.N. Aiyar, O.H. Houwen, and F.W. Bachelor, Fuel, 59(4), 276(1980).
18. W.J. Parkinson, "Shale-Oil Denitrification by Acid Treating," NTIS Report No. LA-9410-MS, 1975.
19. D.C. Cronauer, R.F. Vogel, and R.A. Flinn, U.S. Patent 4,238,320, 1980.
20. B.D. Prasher, and Y.H. Ma, AIChE J., 23, 303(1977).
21. M. Shimura, Y. Shiroto, and C. Takeuchi, paper presented at the 183rd National ACS Meeting, Las Vegas, 1982.
22. R.E. Baltus, and J.L. Anderson, Chem. Eng. Sci., 38, 1959(1983).
23. W.C. Conner, A.M. Lane, K.M. Ng, and M. Goldblatt, J. Catal., 83, 336(1983).
24. D.C. Cronauer, "Novel Techniques for the Denitrogenation of Shale Oil," final report for DOE Contract DE-AC17-80BCI0313, 1984.
25. T. Vermeulen, M.D. LeVan, N.K. Hiester, and G. Klein, "Section 16: Adsorption and Ion Exchange," in Chemical Engineers' Handbook, 6th ed., D.W. Green, ed., McGraw-Hill, NY, 1984.
26. T. Vermeulen, Ind. Eng. Chem., 45(8), 1664(1953).
27. K.R. Hall, L.C. Eagleton, A. Acrivos, and T. Vermeulen, Ind. Eng. Chem. Fundam., 5(2), 212(1966).
28. R. Aris, Ind. Eng. Chem. Fundam., 22(1), 150(1983).
29. Y. Takeuchi, E. Furuya, and H. Ikeda, J. Chem. Eng. Japan, 17(3), 304(1984).